NANO LETTERS

pubs.acs.org/NanoLett Letter

Thousand-fold Increase in Plasmonic Light Emission via Combined Electronic and Optical Excitations

Longji Cui,[▽] Yunxuan Zhu,[▽] Peter Nordlander, Massimiliano Di Ventra, and Douglas Natelson*

Cite This: *Nano Lett.* 2021, 21, 2658−2665 Read Online

ACCESS | Metrics & More | Article Recommendations | Supporting Information

ABSTRACT: Surface plasmon enhanced processes and hot-carrier dynamics in plasmonic nanostructures are of great fundamental interest to reveal light−matter interactions at the nanoscale. Using plasmonic tunnel junctions as a platform supporting both electrically and optically excited localized surface plasmons, we report a much greater (over 1000×) plasmonic light emission at upconverted photon energies under combined electro-optical excitation, compared with electrical or optical excitation separately. Two mechanisms compatible with the form of the observed spectra are interactions of plasmon-induced hot carriers and electronic anti-Stokes Raman scattering. Our measurement results are in excellent agreement with a theoretical model combining electro-optical generation of hot carriers through nonradiative plasmon excitation and hot-carrier relaxation. We also discuss the challenge of distinguishing relative contributions of hot carrier emission and the anti-Stokes electronic Raman process. This observed increase in above-threshold emission in plasmonic systems may open avenues in on-chip nanophotonic switching and hot-carrier photocatalysis.

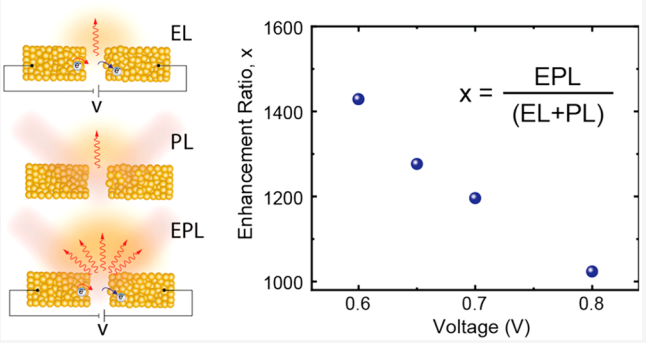

KEYWORDS: *Plasmonics, light emission, tunnel junction, hot-carrier dynamics, synergistic effect*

INTRODUCTION

Optically excited localized surface plasmons (LSPs) in metal nanostructures have been studied extensively and hold promise for technologies including surface-enhanced spectroscopies,[1,2] photosensing,[3,4] photocatalysis,[5−7] and photovoltaics.[8] In recent years progress has also been made in understanding electrically generated LSPs and optical nanoantenna effects,[9−11] opening the potential for plasmonic applications controlled by electronic means. Plasmonic tunnel junctions emerge as a unique experimental platform that supports LSPs generated by both electrical and optical excitations,[10−15] strongly confined in an ultrasmall nanogap. In electrically driven tunnel junctions, electrons tunneling from source drain inelastically excite LSPs,[16,17] which subsequently undergo rapid relaxation via radiative or nonradiative decay.

Recent studies[18−23] of plasmonic light emission in tunnel junctions have reported a strong upconversion effect, with generated photon energy ($\hbar\omega$) significantly above the energy threshold of the incident electrons (eV, where V is the applied bias). While multiple processes can produce such above-threshold photons, recent work[24,25] has revealed the dominant role of LSP-induced hot carriers for this. Similarly, upconversion photoluminescence ($\hbar\omega > \hbar\omega_{exc}$, where $\hbar\omega_{exc}$ is the excitation photon energy) from plasmonic nanoparticles[26−29] has also been observed, and this phenomenon can be explained by mechanisms such as hot-carrier luminescence,[26] anti-Stokes electron Raman scattering,[27,30,31] and other surface-enhanced anti-Stokes processes.[32−34] While previous studies have focused on driving plasmonic nanostructures using either electrical or optical excitation alone and provided insight into the relevant hot-carrier dynamics, the effects of multiple excitation sources remain less explored. A recent work[35] has reported that under electrical and optical excitations, light emission from a Au junction is enhanced as much as 6-fold (total photon counts divided by the simple sum of photons emitted under each excitation). However, such enhancement is driven by the optical interband transition of Au, which generates only below-threshold photons (i.e., photon energy is below the excitation energy). These findings raise the question: Is it possible to excite the system via concurrently applied electronic and optical drive into a regime such that upconversion processes dominate the plasmonic response?

In this work, we report a large increase in upconverted photon emission when simultaneous optical and electrical

Received: February 4, 2021
Revised: March 7, 2021
Published: March 12, 2021

https://dx.doi.org/10.1021/acs.nanolett.1c00503
Nano Lett. 2021, 21, 2658−2665

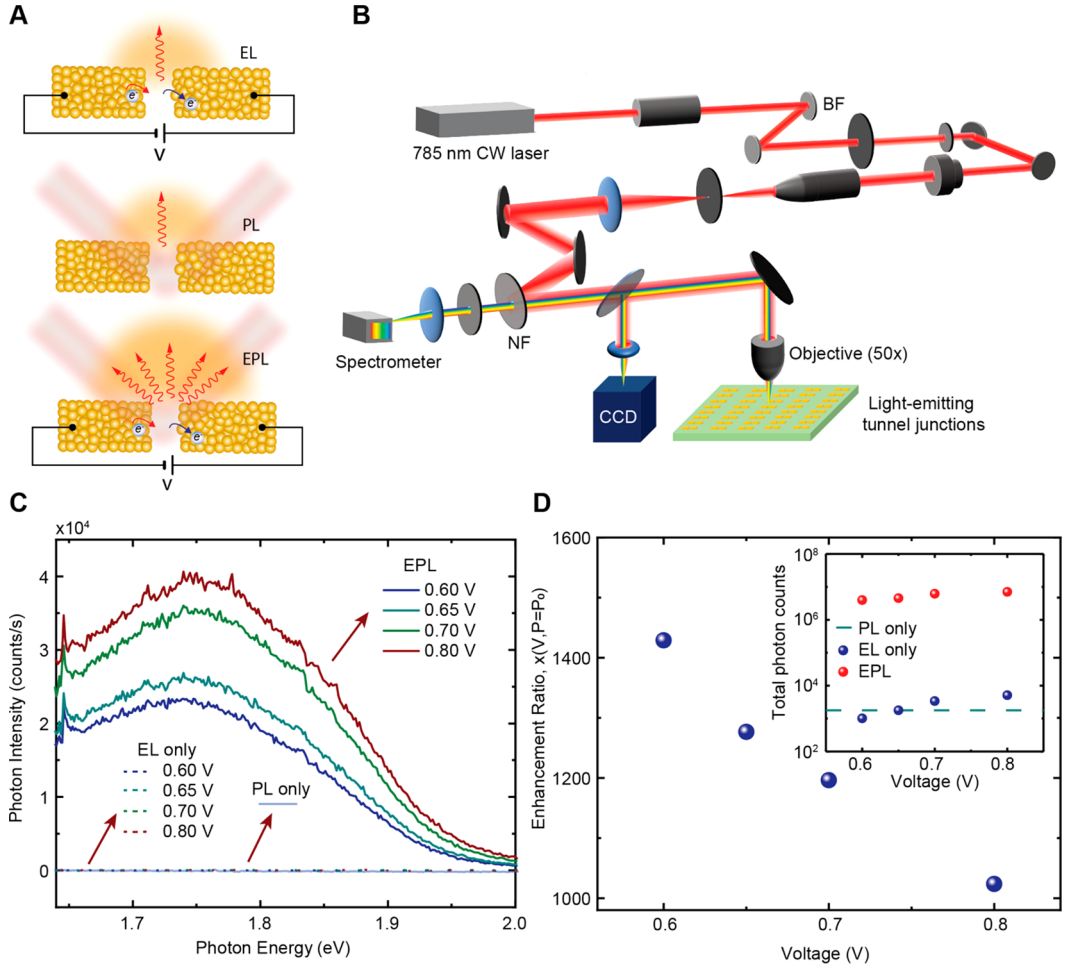

Figure 1. Experimental strategy and observation of the giant increase in upconversion light emission from plasmonic tunnel junctions. (A) Schematics of the experimental design to measure light emission under three types of external stimuli (EL, electroluminescence; PL, photoluminescence; EPL, electro-photoluminescence). (B) Schematics of the combined electrical-optical setup. BF, Bragg filter; NF, Notch filter. The diameter of the focused laser beam through the 50× objective is 1.8 μm. (C) Spectral emission intensity of EL, PL, and EPL for photon energy larger than the energies of both the laser photons and tunneling electrons in a Au junction. The small peaks on EPL between 1000 and 1800 cm^{-1} (~1.7−1.8 eV) are anti-Stokes SERS emission of residual contaminant organic molecules on the sample. The applied laser power in PL and EPL is 0.345 mW. (D) Measured enhancement ratio (total upconverted photons in EPL divided by the sum of EL and PL measured in (C) versus the applied bias with a fixed incident light power of 0.345 mW. The inset shows the total photon counts for EL, PL, and EPL at different biases. The photon count of PL is indicated by the dashed line.

excitations are applied to plasmonic junctions. In Au devices, we found that electrically biased, optically pumped junctions emit over 1000× more upconverted photons than the simple sum of emission under either an electrical or optical stimulus alone (Figure 1A), demonstrating a broadband plasmonic switchable light source controlled by electrical voltage or input optical power. This increase is not just a case of dividing by a small denominator; in the electrically and optically pumped junctions, the above-threshold photons are a majority of the total emission. Analysis of the emission spectra with and without optical pumping reveals that the possible mechanisms involved in this increase are (1) joint production of hot carriers, manifested microscopically as an increase in the effective temperature of the steady-state hot carriers with the addition of optical excitation, and (2) anti-Stokes electronic Raman scattering, with the applied bias and local wave functions setting the phase space for Raman processes.

EXPERIMENTAL RESULTS

The combined optoelectronic experimental setup is shown in Figure 1B. We fabricate arrays of Au nanowires and obtained tunnel junctions by employing the electromigration break junction (EBJ) technique. (see the Supporting Information Sections 1 and 2 for the nanofabrication and electromigration procedure). Subsequent to the creation of the tunneling gaps, light emission measurements were conducted on each junction under three conditions (voltage bias with no incident light; continuous wave (CW) optical excitation at 785 nm with no voltage bias; and optical excitation in the presence of voltage bias), producing electroluminescence (EL), photoluminescence (PL), and electro-photoluminescence (EPL), respectively (Figure 1A).

Figure 1C shows the light emission spectra ($\hbar\omega > \hbar\omega_{exc} \approx$ 1.58 eV) measured from a Au junction. In the EL case, above-threshold emission can be generated via multielectron interactions in the low current limit (~100 nA),[19] and hot-carrier recombination in the high current limit (~100 μA).[24] For PL at zero bias, in addition to the hot-carrier[26] or

https://dx.doi.org/10.1021/acs.nanolett.1c00503
Nano Lett. 2021, 21, 2658−2665

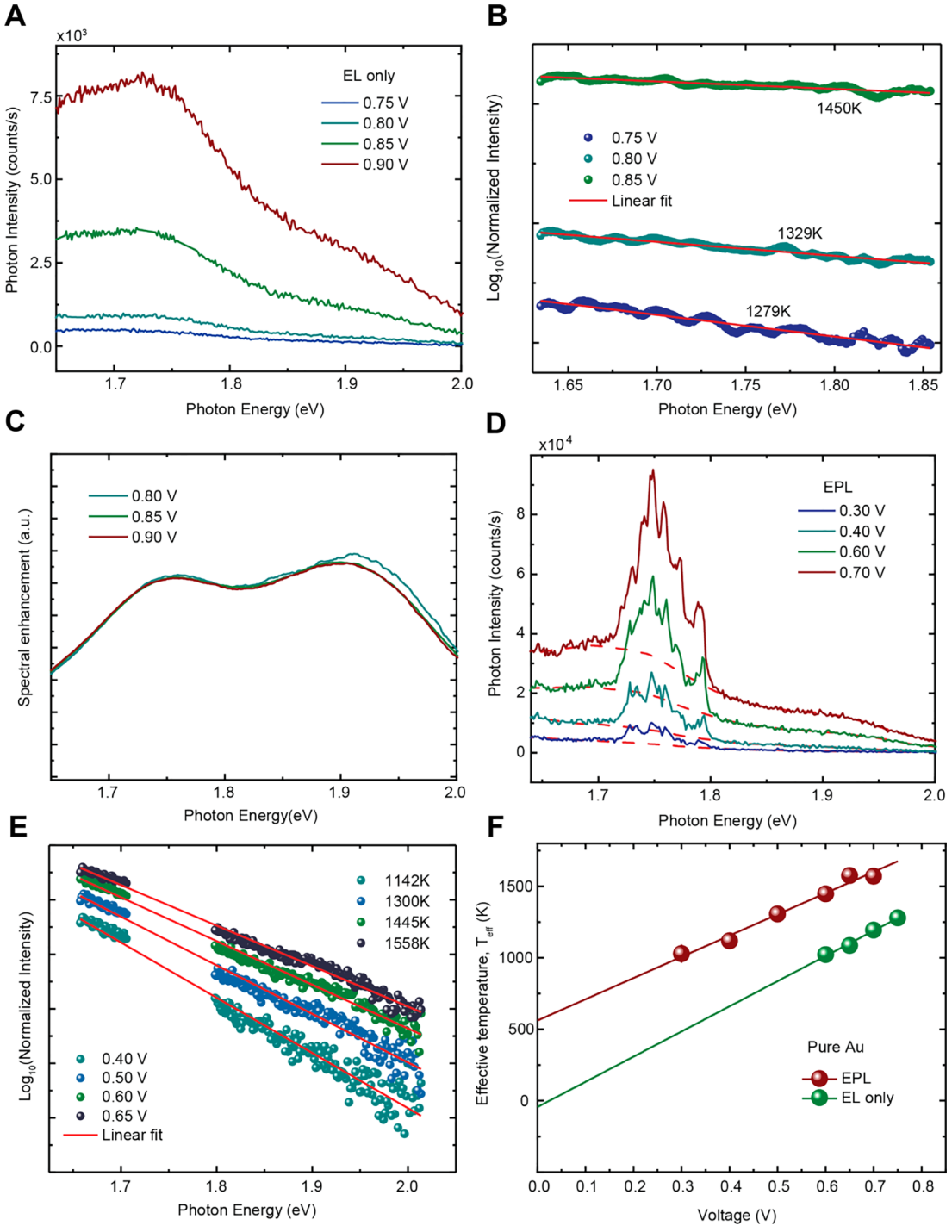

Figure 2. Measurement and analysis of voltage-dependent upconversion light emission. (A) Spectral emission for an electrically driven Au junction (EL only) at different biases. (B) Normalization analysis of the spectra in (A) (spectra at 0.75, 0.80, and 0.85 V are normalized by the spectrum at 0.90 V). The linear decay of the reduced spectra with energy, plotted on a log scale, is fitted with a Boltzmann distribution, $e^{-\hbar\omega/k_B T_{eff}}$, where T_{eff} is the effective temperature of hot carriers. (C) Extracted voltage-independent plasmonic function of the junction from (B). (D) Measured EPL for the same junction at different biases. The incident laser power is 0.46 mW. The dashed red lines correspond to pure EPL excluding the contaminant anti-Stokes SERS contribution. (E) Normalization analysis of EPL spectra, by dividing the spectra in (D) by the plasmonic function in (C). Red lines represent the linear fit with the Boltzmann distribution. The energy range with significant SERS was excluded. (F) Inferred T_{eff} for EPL (red) and EL (green) versus the applied voltage. The lowest measurement voltage (0.6 V for EL and 0.3 V for EPL) is limited by the noise level of the CCD spectrometer. Error bar represents the standard deviation of linear fit in (E).

intraband transition[36] induced photoluminescence, tunneling electrons can also undergo a Raman process (electronic Raman scattering, ERS) before emitting a photon with a different energy.[30,31] As shown in the discussion below, the anti-Stokes emission for the unbiased ERS is mainly due to the thermally excited tail of the electron−hole joint distribution and density of states[31] and thus cannot extend to large wavenumbers beyond $k_B T$. Hence, both EL at low bias and PL can emit only

https://dx.doi.org/10.1021/acs.nanolett.1c00503
Nano Lett. 2021, 21, 2658−2665

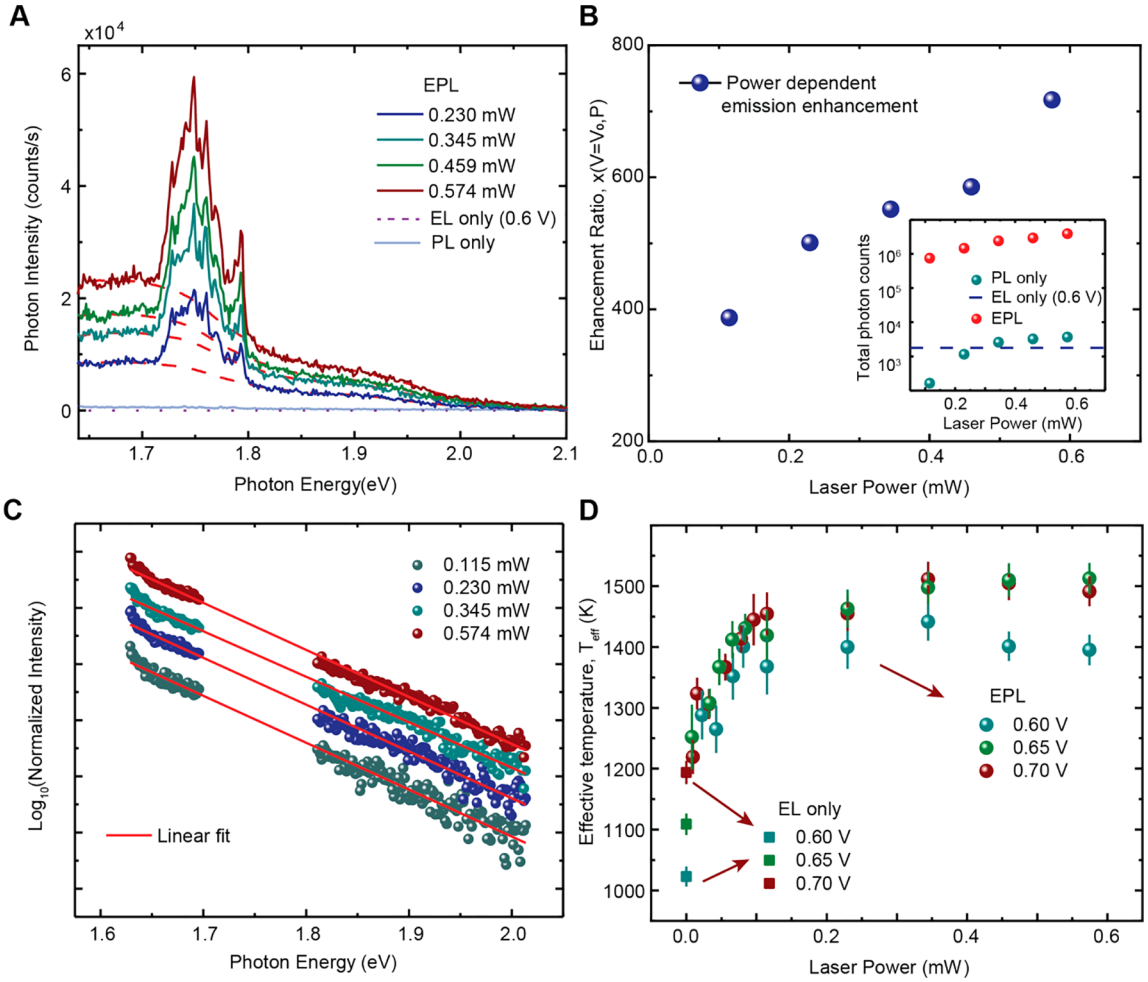

Figure 3. Measurement and analysis of power-dependent upconversion light emission in Au junctions. (A) Spectral light emission for EL, PL, and EPL at different laser power. Dashed red lines are the pure EPL spectra excluding contaminant anti-Stokes SERS contributions. (B) Measured enhancement ratio versus power for light emission recorded in (A) with applied bias V_0 = 0.6 V. The inset shows the calculated total photon counts for EL, PL, and EPL, respectively. The photon count of EL is indicated by the dashed line. (C) Normalization analysis of the power-dependent light emission spectra in (A). Red lines represent the linear fit with a Boltzmann distribution of hot carriers from which the effective temperature of hot carriers can be extracted. The anti-Stoke SERS portion has been removed in this analysis. (D) Inferred power-dependent effective temperature and comparison with the effective temperature obtained for EL under the same voltage bias. Error bars represent the standard deviation of the linear fits in (C).

a few photons at upconversion photon energies, as indicated in Figure 1C. Surprisingly, the junction under simultaneous optical and electrical excitation (EPL) emits far more light than when driven at the individual EL and PL excitation. In the following discussion, we define the enhancement ratio as

$$x(V, P) = \int_{1.65\text{eV}}^{2\text{eV}} U^{\text{EPL}}(\omega, V, P)\, \mathrm{d}\omega \Big/ \int_{1.65\text{eV}}^{2\text{eV}} [U^{\text{EL}}(\omega, V, P = 0) + U^{\text{PL}}(\omega, V = 0, P)]\, \mathrm{d}\omega \quad (1)$$

where P is the optical power and 2.0 eV is chosen as the upper bound of the integral since little light was seen emitted from the junction above this energy, corresponding to the interband transition of Au. As shown in Figure 1D, EPL generates over 1000 times more photons than the total amount of photons generated by the sum of EL and PL. This is a dramatic demonstration that electrical and optical excitation work in cooperation in the upconversion emission process. To verify the reproducibility of this increase in emission, we measured in total 14 pure Au junctions.

Since multiple mechanisms could be contributing to the observed EPL, we will first focus on presenting the experimental results of EPL under different experimental conditions and then discuss the underlying microscopic processes. We performed measurements and analysis of the upconversion emission spectra, the enhancement ratio $x(V, P)$, and their dependence on the applied voltage, laser power, and plasmonic materials. Figure 2 shows the results for a Au junction under different biases without (Figure 2A) and with (Figure 2D) incident power at 0.46 mW. Our past work[24] on light emission from electrically driven junctions shows that, using a normalization method, one can separate the voltage-independent LSP spectrum, $\rho(\omega)$. Here, we perform a similar analysis (see SI Section 6 for details) on the spectra in Figure 2. We first analyze the EL results in the high current limit (Figure 2A, ~20 μA) by normalizing the measured spectra at 0.75, 0.80, and 0.85 V to the spectrum at 0.90 V. Figure 2B shows the reduced spectra, plotted on log scale, in which the

https://dx.doi.org/10.1021/acs.nanolett.1c00503
Nano Lett. 2021, 21, 2658−2665

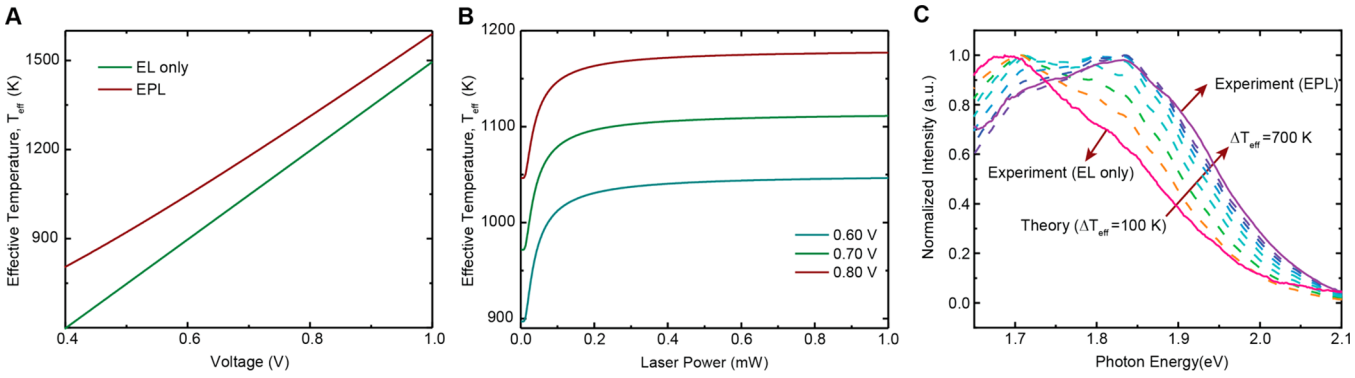

Figure 4. Theoretical modeling of upconversion light emission. (A) Calculated voltage dependence of the effective temperature of hot carriers in EL (green) and EPL (red) cases. (B) Calculated optical power dependence of the effective temperature of hot carriers in EPL at different bias voltages. (C) Starting from the experimentally measured EL spectrum (red), the inferred plasmon spectral shape is combined with Boltzmann factors of increasing T_{eff} (calculated dashed curves). The calculated spectra blue shift and match the experimental EPL spectrum (purple solid curve) with a sufficiently large increase in effective temperature.

normalized log spectral intensity linearly decreases with the photon energy. In our previous work,[24] we used a voltage-dependent effective temperature T_{eff} in a Boltzmann factor, $e^{-\hbar\omega/k_B T_{eff}}$, to parametrize this exponentially decaying trend. The concept of an effective temperature has also been introduced below to interpret the measured EPL.

Following the above analysis, T_{eff} at different biases for EL can be extracted by linearly fitting the reduced spectra to the Boltzmann form. With the T_{eff}, we can then infer back to the underlying LSP contribution $\rho(\omega)$ of the junction from emission spectrum. As shown in Figure 2C, $\rho(\omega)$ obtained from spectra at different voltages collapse to a single curve, confirming that the plasmonic resonances are an intrinsic property of the specific junction, independent of external stimuli.

We then proceed to analyze the measured EPL results from the same junction under optical illumination. By dividing the EPL spectra (the dashed red lines in Figure 2D excluding the SERS contribution) by the inferred $\rho(\omega)$ from Figure 2C, we can test for and obtain a similar exponential dependence. The resultant reduced spectra plotted on log scale (excluding the anti-Stokes SERS of organic contaminants) (Figure 2E) again show clear linear frequency dependence, similar to that obtained in EL (Figure 2B), indicating that an effective temperature can still be used as a parameter to describe the EPL of tunnel junctions.[26]

In Figure 2F, we plot the relation between the applied bias and the extracted T_{eff} of both EL and EPL in the Au junction. We can see that in both EL and EPL, T_{eff} found from the Boltzmann analysis increases linearly with the applied bias. Moreover, a significantly higher T_{eff} is found in the presence of optical pumping (EPL) than the T_{eff} in the EL-only case. Linearly extrapolating the EPL-inferred T_{eff} data down to zero bias (EPL → PL), we find a nonzero T_{eff} at this limit (~500 K in Figure 2F). In contrast, extrapolating the EL-inferred T_{eff} data toward zero bias yields T_{eff} ($V \to 0$) close to 0. The Boltzmann factor and the large difference in T_{eff} between EPL and EL are the reason for the giant synergistic increase in upconversion emission in this hot-carrier picture. By contrast, control experiments using a thin (~1 nm) Cr adhesion layer as a damping medium for the plasmonic response[37] shows a much smaller T_{eff} difference between EPL and EL and a less dramatic increase (< ~10× ; see SI Section 7 for the experimental results of Au/Cr junctions), suggesting that the dramatic increase of upconversion emission in EPL is also closely related to the strength of plasmonic resonance of the materials.

We now focus on the dependence of the EPL on the optical power in tuning the increased emission and influencing the effective temperature. Figure 3A shows the results of the emission spectra for an Au junction under fixed bias $V = 0.6$ V and varying optical power. As expected, higher excitation power induces stronger light emission. Moreover, $x(V = 0.6\ \text{V}, P)$ increases with P, reaching over 700 for relatively small laser power (<1 mW), as shown in Figure 3B.

We performed the normalization analysis to extract the T_{eff} for different P, with $\rho(\omega)$ obtained by the same analysis for the EL spectrum described above. It can be seen from Figure 3C that the logarithmic normalized intensity again exhibits excellent linearity with photon energy. Plotting all extracted T_{eff} at different biases and power (Figure 3D), we reveal a nonlinear power dependence of T_{eff}, in strong contrast to the linear relation between T_{eff} and applied bias (Figure 2E and 2F). Moreover, we find that T_{eff} increases with laser power rapidly and saturates to a voltage-dependent value. These observations, combined with the measured increase effects shown in Figure 3B and Figure 1D, suggest a nontrivial role of combined optical and electrical excitations.

DISCUSSION

We proceed to consider the physical mechanisms behind the observed light emission increase. Here, we discuss two models with distinct microscopic electronic dynamics that can yield the observed exponential dependence on emission energy.

First, following our previous work for EL,[24] we extend the microscopic model based on hot-carrier dynamics to elucidate the mechanism of the observed increase in upconversion emission. We found that the resultant EL spectra can be modeled by

$$U(\omega, V) \propto I^{\alpha}\rho(\omega)e^{-\hbar\omega/k_B T_{eff}} \quad (2)$$

where $\rho(\omega)$ is the LSP contribution, I is the tunneling current, and α is an experimentally extracted value that was found always greater than 1 and indicates the nonlinear current dependence of the above-threshold emission. Note that the hot carriers are not confined only to the drain electrode but are generated throughout the region where the damping of LSPs occurs.[38]

https://dx.doi.org/10.1021/acs.nanolett.1c00503
Nano Lett. 2021, 21, 2658−2665

A more detailed treatment[39] looks at energy dissipation and transport of hot carriers within the electronic system as a consequence of the electronic viscosity at high current density, obtaining the same voltage dependence of the effective temperature ($T_{\text{eff}} \propto V$) (see SI Section 8 for the detailed derivation of the model and calculation for γ_{e-e}) The effective temperature of hot carriers is given by

$$T_{\text{eff}} = \sqrt{(\gamma_{e-e}V)^2 + T_0^2} \tag{3}$$

where γ_{e-e} is related to the effective electronic viscosity and T_0 is the temperature of background electrons in the electrode. Assuming $T_0 \ll T_{\text{eff}}$, valid in the absence of illumination, we will obtain the linear voltage-dependent effective temperature $T_{\text{eff}} \approx \gamma_{e-e}V$. In previous work,[39] calculation for a Au quantum contact predicts $\gamma_{e-e} \approx 65$ K/V but neglects any possible contribution of electronic coupling to LSPs that would significantly amplify the electronic friction. Using the plasmonic properties of Au[40] and applying the formula to calculate the shear viscosity of an electron fluid,[41] we estimate a revised value of $\gamma_{e-e} \approx 1495$ K/V, which agrees very well with our measurements in Figure 2F (~1600 K/V for EL).

In this picture, under simultaneous optical and electrical excitation, there exists an optically driven additional incoherent temperature T_0 in the electrode. Therefore, T_{eff} will show the interaction between optically and electrically generated hot carriers. We follow the approach of Liu et al.[42] to model the heating process due to optical excitation of LSPs which subsequently decay into hot carriers nonradiatively. Voltage and power dependence for modeled T_{eff} under different excitation condition are plotted in Figure 4A and 4B.

As shown in Figure 4A, T_{eff} under optical excitations shows a nonzero value in the zero-bias limit, consistent with our measurement (Figure 2F). Moreover, the observed nonlinear behavior of power-dependent T_{eff} and the saturation at high power with voltage-dependent saturation value are well reproduced in the model (Figure 4B).

While not meant to be a detailed theoretical treatment of this complex system, this model can also quantitatively predict the upconversion emission spectra, as shown in Figure 4C. Given the measured EL and EPL (peak magnitude normalized; the full spectra without normalization and the comparison with theory are shown in Figure S7) of a Au junction (the solid lines in Figure 4C), it can be seen that by taking the EL-inferred spectral shape ($\rho(\omega)$) and manually increasing T_{eff} in eq 2, the calculated spectrum exhibits a clear blue shift due to the variation of the Boltzmann factor and eventually reaches a near-perfect match with the normalized, measured EPL, further suggesting that both EL and EPL can originate from the same hot-carrier effect. Moreover, we can calculate the EPL spectrum by replacing the effective temperature in the EL spectrum with the effective temperature under combined external stimuli and combining a prefactor extracted from the fitting for the EPL spectrum. The calculated EPL spectrum agrees very well with the measured one, as shown in Figure S7.

Within the hot-carrier model, the generalized formula for EPL/EL/PL we derived enables the numerical estimation of the enhancement ratio (see eqs S15 and S16). The key to the synergistic effect lies in the optically induced incoherent temperature T_0, which induces a slower exponential decay with energy at the same bias and thus enables a more prominent contribution of the LSP resonance, both in shape and amplitude. It can be seen that the cooperative effect will be most pronounced at a (device-dependent) moderate bias, where the saturated T_0 value gives the largest difference in the exponential factor before and after optical illumination, which explains why the enhancement ratio decreases with bias in Figure 1D. Such an optimum bias represents the energy scale where the electrical excitation is comparable to the optical pumping. Although the devices in this work do not possess a high energy conversion efficiency (~10^{-6} or below), we note that further improvement can be readily foreseen by using better plasmonic materials, e.g., single-crystalline Au or Ag,[13] and by employing tunneling devices with high stability under high power.

In addition to the hot-carrier recombination mechanism discussed above, anti-Stokes electronic Raman scattering is also a relevant physical mechanism in illuminated, biased junctions and could result in a similar light emission spectrum. In the anti-Stokes electronic Raman process, an electron above the Fermi level is excited by an incident photon into an intermediate virtual state and subsequently recombines with a hole at a different energy and momentum, resulting in a blue-shifted photon scattered into the far field.[30,31] The electronic crystal momentum change during this process, Δk, is constrained by the energy dispersion in the metal, which greatly suppresses this process in the metallic bulk. However, this constraint is relaxed near the surface of nanostructures, where in real space the energy-dependent overlap of the electronic wave functions results in a transition rate that includes a factor which decays exponentially with the Raman shift:[31]

$$\Gamma(\epsilon) \propto \int f(E)[1 - f(E + \epsilon)]e^{-|2\epsilon/\Delta|}\,dE \tag{4}$$

where $f(E)$ is the Fermi−Dirac distribution for an electron with energy E and Δ is the exponential energy decay that may be estimated from a jellium model. The scattered photon then couples to the localized surface plasmon and results in far field emission. In the absence of a voltage bias, the anti-Stokes emission is limited by the finite carrier temperature of the Fermi−Dirac distributions.

A voltage bias can strongly affect anti-Stokes emission in the electronic Raman process by energetically allowing Raman scattering from electron states at the higher Fermi level electrode to hole states at the lower Fermi level electrode. This can lead to anti-Stokes emission within the scale of the bias window eV but which is exponentially suppressed with the Raman shift on the scale of Δ. In this picture, the exponentially decayed normalization spectrum as a function of photon energy (Figure 2E and 3C) can be considered using eq 4 with a bias-dependent allowed energy.

From the pure electroluminescence data, the hot-carrier emission mechanism clearly takes place in these junctions. Similarly, electronic anti-Stokes Raman scattering has been demonstrated in other systems.[31] Determining the relative contributions of the two mechanisms in the present experiments is challenging, since both predict increased emission under combined excitation and the exponential decay of above-threshold emission as a function of energy. The bias and optical power dependence of the experimental data can provide insights for the different microscopic processes described by these two models. While not conclusive, the observation (Figure 4C) that the electroluminescence spectrum and a modeled change in effective electronic temperature can give the combined EPL spectrum is

https://dx.doi.org/10.1021/acs.nanolett.1c00503
Nano Lett. 2021, 21, 2658−2665

suggestive. Conclusively discerning the respective contributions from these two distinctive mechanisms from CW measurements alone is very challenging and beyond the scope of this work. While the electronic Raman process is prompt,[30] in the hot-carrier recombination process the carrier scattering time is much slower (hundreds of femtoseconds).[26] This difference may allow ultrafast measurements to disentangle the respective contributions of hot-carrier dynamics and bias-assisted anti-Stokes electronic Raman scattering.

Our work provides insight into nontrivial light−matter interactions at the nanoscale, demonstrating that the combination of abundant electronic tunneling and interactions with local plasmonic excitations can generate energetic photons in multiple ways. The experimental strategy employed here and the observation of increased emission under combined electronic and optical excitation opens numerous opportunities in nanophotonic and nanoplasmonic applications such as optical modulation of deep subwavelength plasmonic photon sources and hot-carrier photochemistry.[3,5,43]

■ ASSOCIATED CONTENT

Supporting Information

The Supporting Information is available free of charge at https://pubs.acs.org/doi/10.1021/acs.nanolett.1c00503.

> Nanofabrication and sample preparation; electromigration break junction protocol; experimental setup and measurement procedures; influence of anti-Stokes SERS signal on measured light emission spectra; analysis on the Stokes side spectrum; data processing and normalization analysis; control experiments on Au/Cr junctions; theoretical model of hot-carrier dynamics-induced light emission (PDF)

■ AUTHOR INFORMATION

Corresponding Author

Douglas Natelson − *Department of Physics and Astronomy and Smalley-Curl Institute, Rice University, Houston, Texas 77005, United States; Department of Electrical and Computer Engineering and Department of Materials Science and Nanoengineering, Rice University, Houston, Texas 77005, United States;* orcid.org/0000-0003-2370-9859; Email: natelson@rice.edu

Authors

Longji Cui − *Department of Physics and Astronomy and Smalley-Curl Institute, Rice University, Houston, Texas 77005, United States; Paul M. Rady Department of Mechanical Engineering, University of Colorado, Boulder, Colorado 80309, United States; Materials Science and Engineering Program, University of Colorado, Boulder, Colorado 80309, United States;* orcid.org/0000-0003-0469-3230

Yunxuan Zhu − *Department of Physics and Astronomy and Smalley-Curl Institute, Rice University, Houston, Texas 77005, United States*

Peter Nordlander − *Department of Physics and Astronomy and Smalley-Curl Institute, Rice University, Houston, Texas 77005, United States; Department of Electrical and Computer Engineering and Department of Materials Science and Nanoengineering, Rice University, Houston, Texas 77005, United States;* orcid.org/0000-0002-1633-2937

Massimiliano Di Ventra − *Department of Physics, University of California San Diego, La Jolla, California 92093, United States*

Complete contact information is available at: https://pubs.acs.org/10.1021/acs.nanolett.1c00503

Author Contributions

[▽]L.C. and Y.Z. contributed equally to this work. D.N and L.C. designed the experiment. L.C. and Y.Z. fabricated the devices, conducted the experiment, and modeled the data. M.D. modeled viscous electronic heating in the presence of plasmons, and P.N. theoretically modeled the optically driven hot-carrier system. All authors wrote the manuscript and have given approval to the final version of the manuscript.

Notes

The authors declare no competing financial interest.

■ ACKNOWLEDGMENTS

L.C. acknowledges funding support from the J. Evans Attwell Welch Fellowship and the Smalley Curl Institute at Rice University and the support of the College of Engineering and Applied Science at University of Colorado at Boulder. D.N. and Y.Z. acknowledge the Robert A. Welch Foundation award no. C-1636. P.N. acknowledges the Robert A. Welch Foundation award no. C-1222 and AFOSR award no. FA 9550-15-1-0022. D.N. acknowledges support from NSF ECCS-1704625.

■ ABBREVIATIONS

LSP, localized surface plasmon; EL, electroluminescence; PL, photoluminescence; EPL, electro-photoluminescence

■ REFERENCES

(1) Langer, J.; Jimenez de Aberasturi, D.; Aizpurua, J.; Alvarez-Puebla, R. A.; Auguié, B.; et al. Present and Future of Surface-Enhanced Raman Scattering. *ACS Nano* **2020**, *14* (1), 28−117.

(2) Neubrech, F.; Huck, C.; Weber, K.; Pucci, A.; Giessen, H. Surface-Enhanced Infrared Spectroscopy Using Resonant Nanoantennas. *Chem. Rev.* **2017**, *117* (7), 5110−5145.

(3) Knight, M. W.; Sobhani, H.; Nordlander, P.; Halas, N. J. Photodetection with Active Optical Antennas. *Science* **2011**, *332* (6030), 702−704.

(4) Li, W.; Coppens, Z. J.; Besteiro, L. V.; Wang, W.; Govorov, A. O.; et al. Circularly Polarized Light Detection with Hot Electrons in Chiral Plasmonic Metamaterials. *Nat. Commun.* **2015**, *6*, 8379.

(5) Zhou, L.; Swearer, D. F.; Zhang, C.; Robatjazi, H.; Zhao, H.; et al. Quantifying Hot Carrier and Thermal Contributions in Plasmonic Photocatalysis. *Science* **2018**, *362* (6410), 69−72.

(6) Christopher, P.; Xin, H.; Linic, S. Visible-Light-Enhanced Catalytic Oxidation Reactions on Plasmonic Silver Nanostructures. *Nat. Chem.* **2011**, *3* (6), 467−472.

(7) Cortés, E.; Xie, W.; Cambiasso, J.; Jermyn, A. S.; Sundararaman, R.; et al. Plasmonic Hot Electron Transport Drives Nano-Localized Chemistry. *Nat. Commun.* **2017**, *8*, 14880.

(8) Atwater, H. A.; Polman, A. Plasmonics for Improved Photovoltaic Devices. *Nat. Mater.* **2010**, *9* (3), 205−213.

(9) Bharadwaj, P.; Bouhelier, A.; Novotny, L. Electrical Excitation of Surface Plasmons. *Phys. Rev. Lett.* **2011**, *106* (22), 226802.

(10) Du, W.; Wang, T.; Chu, H.-S.; Nijhuis, C. A. Highly Efficient On-Chip Direct Electronic-Plasmonic Transducers. *Nat. Photonics* **2017**, *11* (10), 623−627.

(11) Kern, J.; Kullock, R.; Prangsma, J.; Emmerling, M.; Kamp, M.; et al. Electrically Driven Optical Antennas. *Nat. Photonics* **2015**, *9* (9), 582−586.

(12) Wang, P.; Krasavin, A. V.; Nasir, M. E.; Dickson, W.; Zayats, A. V. Reactive Tunnel Junctions in Electrically Driven Plasmonic Nanorod Metamaterials. *Nat. Nanotechnol.* **2018**, *13* (2), 159−164.
(13) Qian, H.; Hsu, S.-W.; Gurunatha, K.; Riley, C. T.; Zhao, J.; et al. Efficient Light Generation from Enhanced Inelastic Electron Tunnelling. *Nat. Photonics* **2018**, *12* (8), 485−488.
(14) Leon, C. C.; Rosławska, A.; Grewal, A.; Gunnarsson, O.; Kuhnke, K.; et al. Photon Superbunching from a Generic Tunnel Junction. *Sci. Adv.* **2019**, *5* (5), No. eaav4986.
(15) Parzefall, M.; Bharadwaj, P.; Jain, A.; Taniguchi, T.; Watanabe, K.; et al. Antenna-Coupled Photon Emission from Hexagonal Boron Nitride Tunnel Junctions. *Nat. Nanotechnol.* **2015**, *10* (12), 1058−1063.
(16) Uehara, Y.; Kimura, Y.; Ushioda, S.; Takeuchi, K. Theory of Visible Light Emission from Scanning Tunneling Microscope. *Jpn. J. Appl. Phys.* **1992**, *31*, 2465−2469.
(17) Persson, B. N. J.; Baratoff, A. Theory of Photon Emission in Electron Tunneling to Metallic Particles. *Phys. Rev. Lett.* **1992**, *68* (21), 3224−3227.
(18) Buret, M.; Uskov, A. V.; Dellinger, J.; Cazier, N.; Mennemanteuil, M.-M.; et al. Spontaneous Hot-Electron Light Emission from Electron-Fed Optical Antennas. *Nano Lett.* **2015**, *15* (9), 5811−5818.
(19) Peters, P.-J.; Xu, F.; Kaasbjerg, K.; Rastelli, G.; Belzig, W.; et al. Quantum Coherent Multielectron Processes in an Atomic Scale Contact. *Phys. Rev. Lett.* **2017**, *119* (6), 066803.
(20) Schull, G.; Néel, N.; Johansson, P.; Berndt, R. Electron-Plasmon and Electron-Electron Interactions at a Single Atom Contact. *Phys. Rev. Lett.* **2009**, *102* (5), 057401.
(21) Kaasbjerg, K.; Nitzan, A. Theory of Light Emission from Quantum Noise in Plasmonic Contacts: Above-Threshold Emission from Higher-Order Electron-Plasmon Scattering. *Phys. Rev. Lett.* **2015**, *114* (12), 126803.
(22) Xu, F.; Holmqvist, C.; Belzig, W. Overbias Light Emission Due to Higher-Order Quantum Noise in a Tunnel Junction. *Phys. Rev. Lett.* **2014**, *113* (6), 066801.
(23) Fung, E. D.; Venkataraman, L. Too Cool for Blackbody Radiation: Overbias Photon Emission in Ambient STM Due to Multielectron Processes. *Nano Lett.* **2020**, *20* (12), 8912−8918.
(24) Cui, L.; Zhu, Y.; Abbasi, M.; Ahmadivand, A.; Gerislioglu, B.; et al. Electrically Driven Hot-Carrier Generation and Above-Threshold Light Emission in Plasmonic Tunnel Junctions. *Nano Lett.* **2020**, *20* (8), 6067−75.
(25) Zhu, Y.; Cui, L.; Natelson, D. Hot-Carrier Enhanced Light Emission: The Origin of above-Threshold Photons from Electrically Driven Plasmonic Tunnel Junctions. *J. Appl. Phys.* **2020**, *128* (23), 233105.
(26) Cai, Y.-Y.; Sung, E.; Zhang, R.; Tauzin, L. J.; Liu, J. G.; et al. Anti-Stokes Emission from Hot Carriers in Gold Nanorods. *Nano Lett.* **2019**, *19* (2), 1067−1073.
(27) Hugall, J. T.; Baumberg, J. J. Demonstrating Photoluminescence from Au Is Electronic Inelastic Light Scattering of a Plasmonic Metal: The Origin of SERS Backgrounds. *Nano Lett.* **2015**, *15* (4), 2600−2604.
(28) Neupane, B.; Zhao, L.; Wang, G. Up-Conversion Luminescence of Gold Nanospheres When Excited at Nonsurface Plasmon Resonance Wavelength by a Continuous Wave Laser. *Nano Lett.* **2013**, *13* (9), 4087−4092.
(29) Naik, G. V.; Welch, A. J.; Briggs, J. A.; Solomon, M. L.; Dionne, J. A. Hot-Carrier-Mediated Photon Upconversion in Metal-Decorated Quantum Wells. *Nano Lett.* **2017**, *17* (8), 4583−4587.
(30) Mertens, J.; Kleemann, M.-E.; Chikkaraddy, R.; Narang, P.; Baumberg, J. J. How Light Is Emitted by Plasmonic Metals. *Nano Lett.* **2017**, *17* (4), 2568−2574.
(31) Dey, S.; Banik, M.; Hulkko, E.; Rodriguez, K.; Apkarian, V. A.; et al. Observation and Analysis of Fano-like Lineshapes in the Raman Spectra of Molecules Adsorbed at Metal Interfaces. *Phys. Rev. B: Condens. Matter Mater. Phys.* **2016**, *93* (3), 035411.
(32) Lombardi, A.; Schmidt, M. K.; Weller, L.; Deacon, W. M.; Benz, F.; et al. Pulsed Molecular Optomechanics in Plasmonic Nanocavities: From Nonlinear Vibrational Instabilities to Bond-Breaking. *Phys. Rev. X* **2018**, *8* (1), 011016.
(33) Crampton, K. T.; Fast, A.; Potma, E. O.; Apkarian, V. A. Junction Plasmon Driven Population Inversion of Molecular Vibrations: A Picosecond Surface-Enhanced Raman Spectroscopy Study. *Nano Lett.* **2018**, *18* (9), 5791−5796.
(34) Maher, R. C.; Galloway, C. M.; Le Ru, E. C.; Cohen, L. F.; Etchegoin, P. G. Vibrational Pumping in Surface Enhanced Raman Scattering (SERS). *Chem. Soc. Rev.* **2008**, *37* (5), 965−979.
(35) Wang, X.; Braun, K.; Zhang, D.; Peisert, H.; Adler, H.; et al. Enhancement of Radiative Plasmon Decay by Hot Electron Tunneling. *ACS Nano* **2015**, *9* (8), 8176−8183.
(36) Beversluis, M.; Bouhelier, A.; Novotny, L. Continuum Generation from Single Gold Nanostructures through Near-Field Mediated Intraband Transitions. *Phys. Rev. B: Condens. Matter Mater. Phys.* **2003**, *68* (11), 115433.
(37) Habteyes, T. G.; Dhuey, S.; Wood, E.; Gargas, D.; Cabrini, S.; et al. Metallic Adhesion Layer Induced Plasmon Damping and Molecular Linker as a Nondamping Alternative. *ACS Nano* **2012**, *6* (6), 5702−5709.
(38) Shalem, G.; Erez-Cohen, O.; Mahalu, D.; Bar-Joseph, I. Light Emission in Metal−Semiconductor Tunnel Junctions: Direct Evidence for Electron Heating by Plasmon Decay. *Nano Lett.* **2021**, *21* (3), 1282−1287.
(39) D'Agosta, R.; Sai, N.; Di Ventra, M. Local Electron Heating in Nanoscale Conductors. *Nano Lett.* **2006**, *6* (12), 2935−2938.
(40) Manfredi, G. How to Model Quantum Plasmas. *Fields Inst. Commun.* **2005**, *46*, 263−287.
(41) Di Ventra, M. *Electrical Transport in Nanoscale Systems*; Cambridge Univ. Press: 2008.
(42) Liu, J. G.; Zhang, H.; Link, S.; Nordlander, P. Relaxation of Plasmon-Induced Hot Carriers. *ACS Photonics* **2018**, *5* (7), 2584−2595.
(43) Reddy, H.; Wang, K.; Kudyshev, Z.; Zhu, L.; Yan, S.; et al. Determining Plasmonic Hot-Carrier Energy Distributions via Single-Molecule Transport Measurements. *Science* **2020**, *369* (6502), 423−426.

https://dx.doi.org/10.1021/acs.nanolett.1c00503
Nano Lett. 2021, 21, 2658−2665